Int. J. Solids Structures, 1974, Vol. 10, pp. 685–699. Pergamon Press. Printed in Gt. Britain.

EXPERIMENTAL INVESTIGATION OF NORMAL PERFORATION OF PROJECTILES IN METALLIC PLATES†

J. AWERBUCH‡ and S. R. BODNER§

Department of Materials Engineering,
Technion-Israel institute of Technology, Haifa, Israel

(*Received* 16 *July* 1973; *revised* 30 *November* 1973)

Abstract—This paper describes an experimental program on ballistic perforation of metallic plates. Three kinds of rifles and various steel and aluminum target plates were used. Measurements were made of the initial and post-perforation velocities and in some cases of the time duration of perforation. High speed photographs were taken during the perforation process and detailed studies were made on sections of the perforated target plates. The examination of the physical process of perforation served to motivate aspects of the analytical treatment presented in an associated paper. The experimental results, i.e. post-perforation velocities and duration times, were found to be in good agreement with predictions of the associated analysis.

NOTATION

b plug length
D_1 entrance dia
D_3 exit dia
e radial width of shear zone of the target plate
V_i impact velocity
V_f final velocity
ΔV $V_i - V_f$
$\dot{\gamma}$ shear strain rate
μ coefficient of viscosity for shearing deformation
σ_c dynamic ultimate compressive stress
τ dynamic ultimate shear stress
τ_0 "quasi-static" ultimate shear stress, $\tau = \tau_0 + \mu\dot{\gamma}$.

INTRODUCTION

An analysis of the mechanics of normal perforation of metallic plates by projectiles at ordnance velocities has been presented in an associated paper[1]. The actual physical process of perforation is extremely complex and the analysis attempts only to identify the main features of the process and thereby to formulate the governing equations of motion. In the analysis, the perforation process is considered to consist of three interconnected stages, namely, an initial compression followed by combined compression and formation of a plug and finally the shearing of a plug until the target material fails and the plug is

† The research reported in this paper has been sponsored in part oy the Air Force Office of Scientific Research (AFSC) through the European Office of Aerospace Research, EOAR, United States Air Force under Contract F 44620-72-C-0004.

‡ Lecturer.

§ Professor.

ejected. Among the factors neglected in the analysis are elastic and plastic wave effects and compressibility of the target material.

A preliminary analysis of the ballistic problem[2] had been compared with experimental results with moderate success. That analysis was subsequently modified by Goldsmith and Finnigan[3] who also conducted an extensive experimental program using spherical projectiles over a wide range of impact velocities. The new analysis[1] was motivated in part by various shortcomings and limitations of the previous work[2, 3] indicated by the results of the experimental program described in this paper as well as by the results of[3]. The main modifications to the previous analyses were the consideration of three rather than two stages for the perforation process and a more realistic description of plug formation and the associated shearing process.

The present experimental program was intended to provide detailed information on the perforation process to assist the development of the analysis and to supply results for comparison purposes. In order to obtain a suitable range of results, three rifles, four projectile types, and a variety of steel and aluminum alloy target plates were used. The projectiles were standard ordnance bullets and, since no provision was available to change the powder weight, the velocity of each type of bullet could not be altered. Measurements were taken of the initial and post-perforation velocities and in some cases of the duration time of perforation. High speed photographs were taken at different times after impact. Calculations based on the analysis of[1] were made for all the test conditions in this experimental program and also for a number of the experimental cases described in[3].

EXPERIMENTAL PROCEDURE

The ballistic experiments were performed in a ballistics range that had provision for measurement of the initial and post-perforation velocities of the projectile and for taking a single high speed photograph of the perforation process. A schematic of the system is shown in Fig. 1.

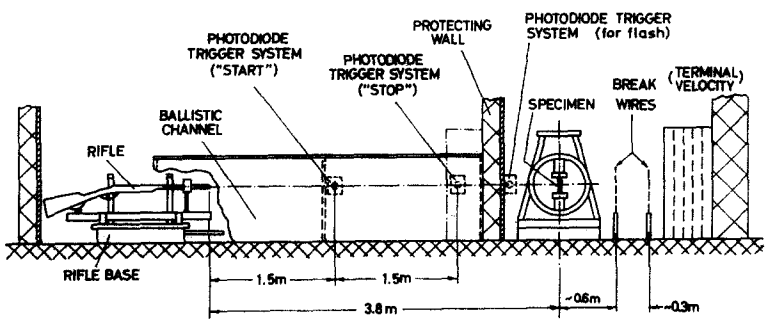

Fig. 1. Schematic of the ballistic range.

The initial velocity was measured by photodiode systems at two stations which were connected to a microsecond interval counter. The post-perforation velocity of the projectile was measured by two wire grid break circuits coupled to another microsecond interval counter. This was necessary due to deviations of the path of the bullet after perforation. The target plate was kept in a darkened room with a camera with an open shutter focused on the impact region. A single photograph could be taken during each test by triggering a light flash at an appropriate time delay after the projectile passed a photodiode station.

The light flash was of 3 μsec duration obtained by a General Radio Type 1531 Strobotac. This was triggered by a Monsanto Pulse Generator, Model 302A, which includes an electronic delay unit. By repeating tests of similar projectiles and target plates with different delay times, a sequence of photographs for the full perforation process could be obtained. Because of small variations in the impact velocities for the different tests, the time interval between the photographs could not be determined exactly. However, by noting those cases of almost identical impact velocity, approximate values for the time intervals between photographs could be estimated.

The rifles used in the program were a standard 7·62 mm caliber military rifle, a 0·22 in. caliber sport rifle, and a 9 mm semi-automatic gun. Regular lead bullets were used and, in addition, armour piercing bullets for the standard military rifle. The properties and velocities for the various projectiles are listed in Table 1. The target plates consisted of a number of high strength steel alloys, mild steel, commercially pure aluminum, and an aluminum alloy. The mechanical properties and thicknesses of the target plates are listed in Table 2. The plates had dimensions 250 × 250 mm and were clamped in a rigid support along two opposite edges. Impact occurred at the midpoint.

Table 1. Projectile data

Rifle type	Projectile type	Projectile symbol	Projectile dia (mm)	Projectile muzzle velocity (m/sec)	Projectile weight (g)	Projectile kinetic energy (m kg)
Standard	Regular-lead	S.-R.	7·62	850	9·30	343
Standard	Armour-piercing	S.-A.P.	7·62	850	9·81*	361
0·22 in. cal.	Regular-lead	TT.-R.	5.6	400	2·63	21·4
9 mm cal. Automatic	Regular-lead	A.-R.	9·0	420	7·40	66·5

* core weight = 3·7 grams

The time duration of the perforation process was measured in a few of the tests. This was achieved by break circuits consisting of fine wires bonded to the plate at the impact and exit points. Impact caused the first wire to break giving an initial signal. The ejection of the plug from the plate provided the terminal signal for the process. The signals were recorded on a dual channel oscilloscope (Tektronix R5030). This method of measuring the duration time is compatible with the computation of the time given in[1]. In practice, the procedure proved to be inaccurate on some occasions due to fusing of the projectile and the plug, so a number of tests (8–10) were run for each case to obtain reliable measurements.

EXPERIMENTAL RESULTS

A typical sequence of photographs for the perforation process is shown in Fig. 2. This sequence was for the case of regular lead bullets (29 mm long) from a standard military rifle penetrating 19·0 mm thick 6061-T6 aluminum alloy plates. The approximate times after impact are indicated on some of the photographs. The times were too uncertain for those that do not have a time designation. These and similar photographs were very helpful in the analytical formulation of the perforation process described in[1].

Some immediate observations can be drawn from these photographs. For example, it is seen from photograph (*f*) that the bullet is completely embedded in the plate just as motion

Table 2. Mechanical properties of target materials

Target material	Target thickness (mm)	Symbol	Yield stress‡ (kg/mm²)	Ultimate stress‡ (kg/mm²)	Ultimate shear stress§ (kg/mm²)	Hardness
Steel Alloy A	6·0 8·0	SA-A-6 SA-A-8	98	110	65	35 Rc
Steel Alloy B	6.35	SA-B-6·35	120	150	80	45 Rc
Steel Alloy C	8·0	SA-C-8	105	132	70	42 Rc
Steel Alloy D	9·0 10·0 12·0 16·0	SA-D-9 SA-D-10 SA-D-12 SA-D-16	90	120	60	38 Rc
Mild Steel	10·0	MS-A-10	28	45	18	109 BHN†
Aluminum 1100-H14	1·0 2·0 3·0 4·0 5·0 6·0	AL-1-1 AL-1-2 AL-1-3 AL-1-4 AL-1-5 AL-1-6	12	12·7	7·7	32 BHN†
Aluminum 6061-T6	1·0 2·0 3·0 3·5 5·0 6·35 9·6 13·1 19·0	AL-6-1 AL-6-2 AL-6-3 AL-6-3·5 AL-6-5 AL-6-6·35 AL-6-9·6 AL-6-13·0 AL-6-19·0	26 — 28 28	29·5 32 32 32	19·0 21	90 BHN† 90 BHN†

† 500 KG load mm ball.
‡ Quasi-static tension.
§ Based on literature data for specified material.

of the rear surface commences. This implies that appreciable flattening of the projectile takes place. The onset of motion of the rear surface, photograph (*f*), is the condition for the start of stage 3 of the perforation process as outlined in[1]. Stage 3 therefore starts about 29 μsec after impact for this case. This stage would end once the plug starts to eject which would correspond to sometime between photographs (*f*) and (*g*). The duration of the third stage was measured from the photographs to be about 2 μsec which is much shorter than the time to the start of the last stage. This short time corresponds, in general, to results calculated on the basis of the analysis[1]. The total time for the perforation process to be completed, i.e. the time from initial impact to ejection of the plug, is estimated from the photographs to be 50 μsec while the calculations give 57 μsec. The more exact contact wires for experimental measurement of the duration time were not used for this case.

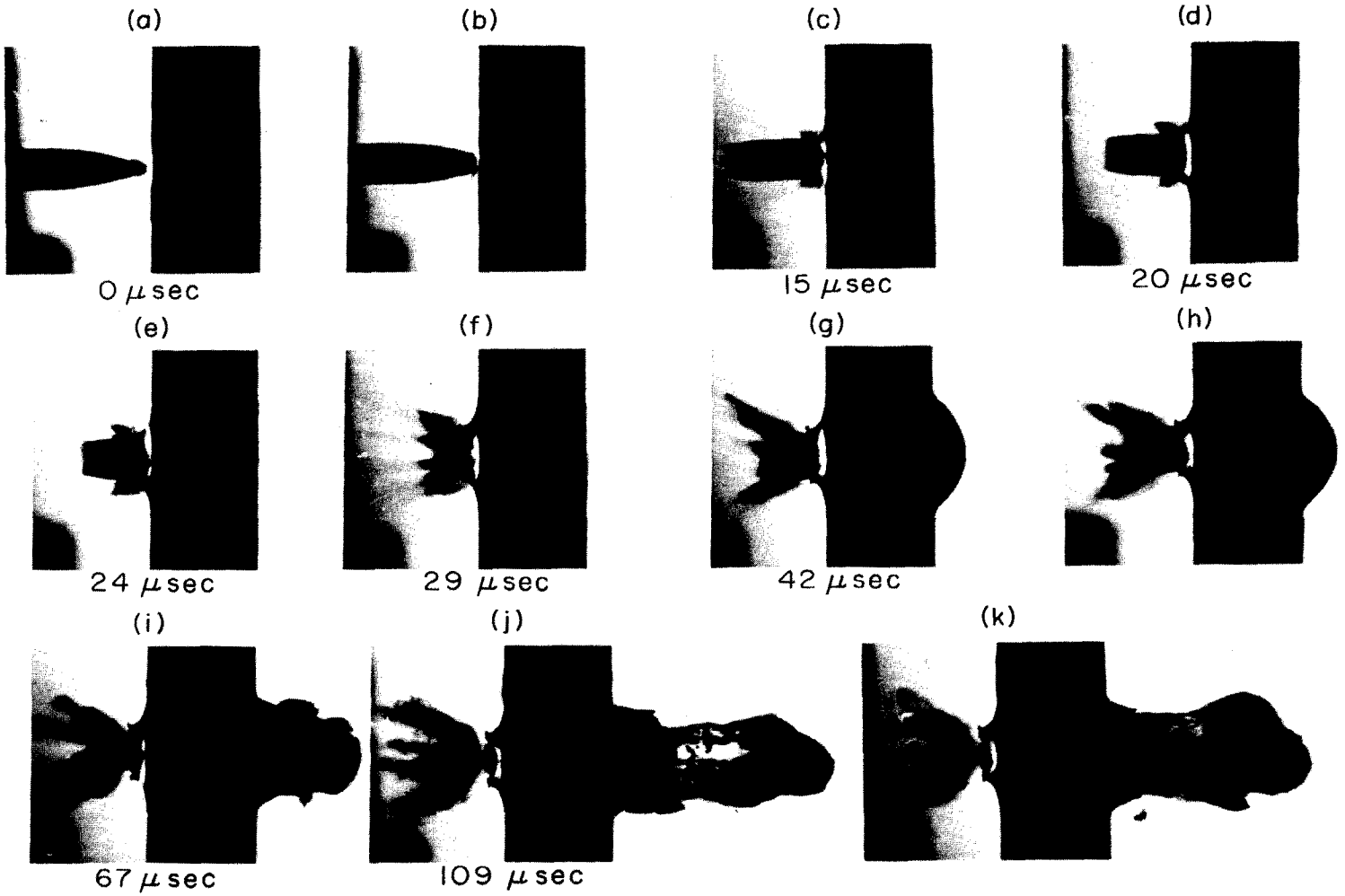

Fig. 2. Photographic sequence showing the perforation process of regular rifle (S.-R.) bullets in aluminum 6061-T6 target plate 19.0 mm thick.

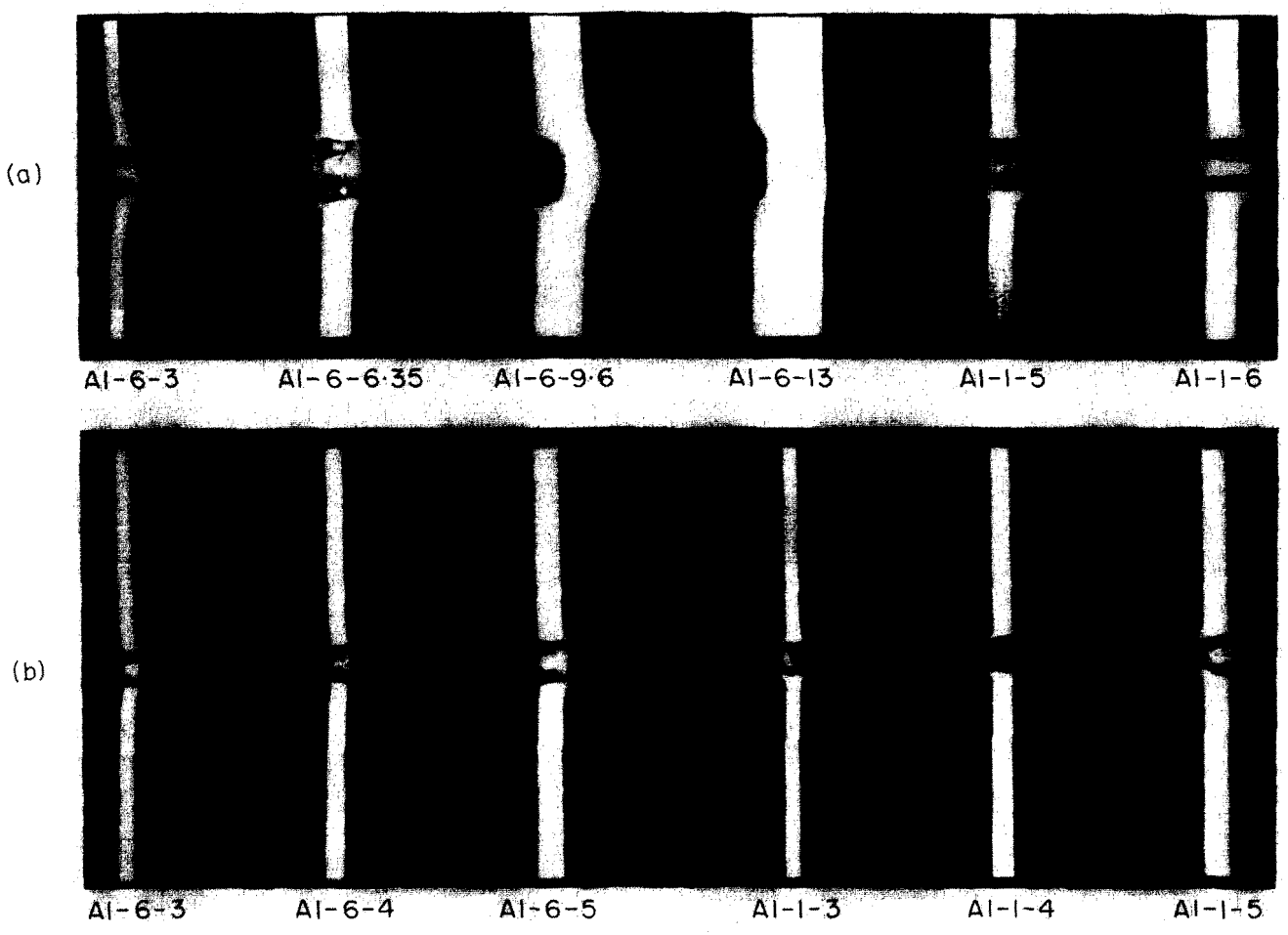

Fig. 3. Cross-sections of commercially pure aluminum and aluminum 6061-T6 plates perforated by (a) A.-R. projectiles and (b) TT.-R. projectiles.

Another observation from the photographs is that the rear surface of the plate rapidly acquires the terminal velocity of the projectile once it is set into motion. This implies that the distance the plug moves before shear failure occurs is small, which is consistent with the analysis. The third stage is therefore completed while the projectile is still embedded in the target plate. The ejected plug and the projectile then both travel at the terminal velocity and in some cases are fused together. In a few cases, however, fragments of the plug and projectile were ejected at higher velocities which disturbed the measurement of the post-perforation velocity.

Typical cross-sections of perforated plates are shown in Fig. 3. The cavities are almost completely cylindrical in most of the cases. In some cases the cavity diameter increases linearly with depth after an initial penetration which corresponds to the first (compressive) stage of the process. The two photographs for the cases where the projectile did not perforate indicate that the projectile was stopped during the third stage since bulging of the rear surface is observed.

A number of the perforated plates were etched and photomicrographed in order to obtain more detailed information on the perforation process. Etching of original plates reveals "flow" lines running parallel to the plate surfaces due to the rolling operation. These flow lines serve as a useful reference grid to analyze deformations due to perforation.

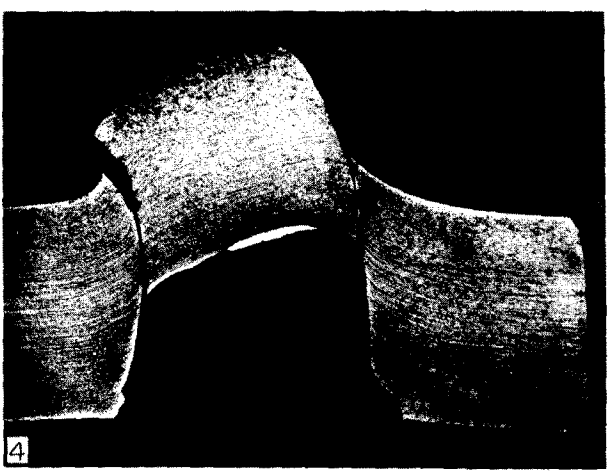

Fig. 4. Photomicrograph of etched SA-D-10 plate after perforation by S.-R. projectile.

Typical photomicrographs of etched perforated specimen plates are shown in Figs. 4–7. The case shown in Fig. 4 is one in which the plug was not fully ejected. This is rarely observed and serves as a convenient illustration of the three stages of perforation described in the analysis. Both Figs. 4 and 5 give good indications of the depth of the first (compression) stage. The flow lines are hardly distorted to that depth so shear effects would be small in that stage (as had been assumed). The flow lines in Figs. 4 and 5 are appreciably distorted in the vicinity of the plug interface which indicates that shear deformation is the dominant mechanism for plugging (stages 2 and 3).

A cross-section where the projectile did not perforate the plate is shown in Fig. 6. Since the rear surface bulges slightly, the process was terminated at the onset of the third stage. The flow lines show some distortion in the region of incipient plugging indicating the

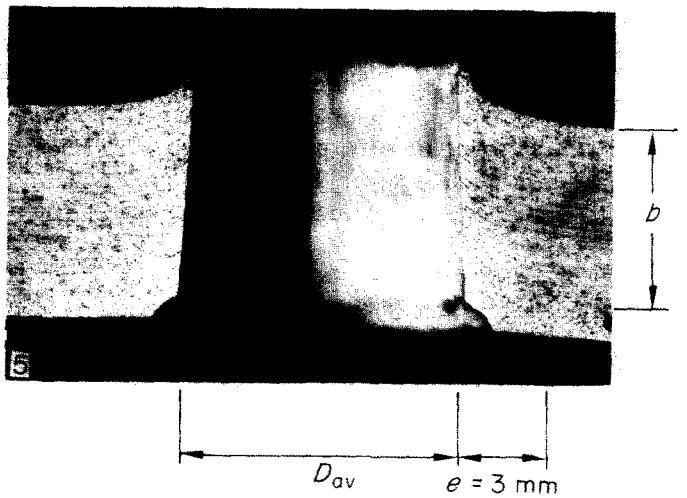

Fig. 5. Photomicrograph of etched SA-C-8 plate after perforation by S.-R. projectile.

existence of shear effects during the second stage. However, the total shear strain accumulated during that stage is seen to be relatively small compared to the cases where perforation occurs, e.g. Figs. 4 and 5. The assumption in the analysis that the shear strain developed during stage 2 can be neglected compared to that of stage 3 appears to be reasonable from these photographs.

Fig. 6. Photomicrograph of etched SA-D-12 plate after penetration by S.-R. projectile.

A parameter that appears in the equations of motion for stages 2 and 3 is the radial width of the shear zone, e. This can be obtained from the photographs as the radial distance from the plug interface to the point where the flow lines start to curve. The point is somewhat arbitrary but the final calculated results are not sensitive to the exact value of e. Values for e for Figs. 5 and 7 are indicated next to the photographs and were used in the calculations for the second stage. In cases where the cavity diameter changes with depth, e.g. Fig. 7, the value of e changes as well and an average value for e was used. The flow lines tend to

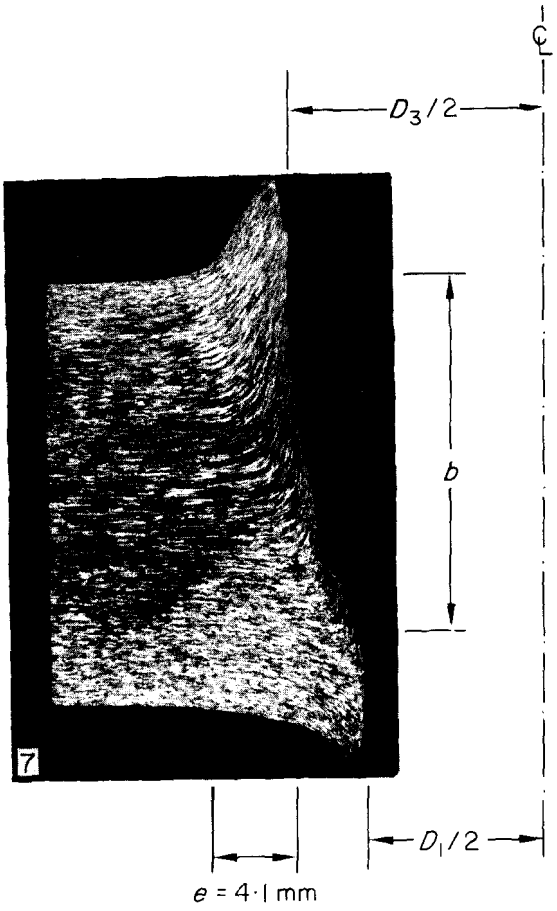

Fig. 7. Photomicrograph of etched AL-6-19 plate after perforation by S.-R. projectile.

curve more sharply close to the interface which is an indication that e becomes smaller during the third stage, i.e. the shear effected zone becomes smaller as the shear strain increases. This is readily seen in Fig. 7 and to some extent in Fig. 4. The value of e actually used in the calculations for the third stage was smaller than that measured and used for the second stage in order to ensure force continuity between the stages. A discontinuity in the total force would otherwise occur since the inertial force immediately becomes zero at the onset of the third stage. The characteristics of the flow lines in the photographs, i.e. the small region of large shear deformation near the interface, indicate that a related effect may occur physically.

Figure 7 also shows a relatively large change in the cavity diameter for the second and third stages. When the entrance and exit diameter D_1 and D_3, were appreciably different, the calculations were based on using D_1 for the first stage and the average of D_1 and D_3 for the second and third stages.

The plugs ejected from the plates were recovered and examined. They were generally cylindrical in shape with spherical surfaces at both ends, e.g. Fig. 8. It is interesting to note that the plugs themselves were almost free of shear effects, i.e. the shearing action occurred entirely in the region outside the plug boundary.

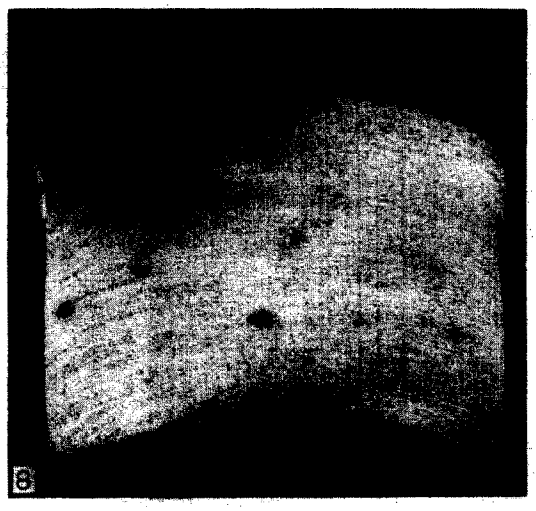

Fig. 8. Photomicrograph of sheared plug of SA-C-8 plate after ejection by S.-R. projectile.

Table 3. Comparison between experimental and theoretically predicted results

Projectile	Target material	Hole dia. D_{avg} or D_1/D_3 (mm)	Plug length b (mm)	Width of shear zone e (mm)	Velocity (m/sec) Measured Initial (V_i)	Measured Final (V_f)	Computed Final (V_f)	Contact duration Computed (μsec)	Contact duration Measured (μsec)
S.-R.	SA-A-6	10·5	5·0	—	850	500–600‡	453	20·6	26·9
S.-R.	SA-A-8	10·6	6·9	4·5	855	460	318	35·5	36·2
S.-R.	SA-B-6·35	10·4	5·3	3·0	854	350–550	400	23·6	
S.-R.	SA-C-8	10·0	7·0	3·0	855	450–470	351	34·2	27·8
S.-R.	SA-D-9	10·5	7·7	2·2	850	220–290†	243	46·0	
S.-R.	SA-D-10	11·5	8·6	3·0	845	155–185†	95	114·5	
S.-R.	MS-A-10	10·6/13·2	5·8	3·5	855	400	361	32·5	
S.-R.	AL-6-9·6	8·2/8·6	2·5	—	845	748	702	16·0	
S.-R.	AL-6-13·0	8·1/12·1	7·5	3·0	845	712	604	30·2	
S.-R.	AL-6-19·0	8·1/13·9	12·0	4·1	836	568–585	406	57·2	
S.A.P.	SA-A-6	10·5	5·0	—	835	550–650‡	499	19·5	
S.A.P.	SA-B-6·35	9·8	5·0	—	848	500–600‡	492	19·9	
S.A.P.	SA-D-12	9·0/5·9	9·0	5·5	855	300–390	418	42·1	
TT.-R.	AL-1-1	5·9	0·7	—	387	369	367	4·6	
TT.-R.	AL-1-2	6·0	1·4	—	385	346	342	9·6	
TT.-R.	AL-1-3	6·0/6·5	2·2	1·3	397	332	324	15·0	
TT.-R.	AL-1-4	6·00/7·55	2·8	1·2	393	292	287	21·4	
TT.-R.	AL-1-5	6·1/8·55	3·4	1·3	410	275	267	27·3	
TT.-R.	AL-1-6	6·0/9·1	4·2	1·5	387	186	203	39·8	
TT.-R.	AL-6-1	5·8	0·65	—	379	357	355	4·2	
TT.-R.	AL-6-2	6·1	1·5	—	399	341	342	9·8	
TT.-R.	AL-6-3	6·6	2·0	1·4	397	309	299	15·3	
TT.-R.	AL-6-4	7·1	2·5	1·5	389	268	255	20·6	
TT.-R.	AL-6-5	7·8	3·5	1·5	401	174	160	38·1	
A.-R.	AL-1-4	9·05	2·80	1·75	416	355	345	18·6	
A.-R.	AL-1-5	9·3	3·5	2·1	422	339	331	23·8	32·0
A.-R.	AL-1-6	9·45	4·2	2·8	428	330	317	29·4	19·0
A.-R.	AL-6-3	9·6	1·6	1·75	422	349	354	12·2	
A.-R.	AL-6-5	10·3	3·6	1·9	416	291	279	27·3	24·0
A.-R.	AL-6-6·35	10·9	5·0	2·0	412	234	208	44·7	35·0

† Close to ballistic limit. ‡ Fragmentation occurred.

The experimental results for the various tests are listed in Table 3. The information obtained for each test includes the initial and post-perforation velocities, the entrance and exit diameters, D_1, D_3 (given as a single average value if the cavity were essentially cylindrical), the width of the shear zone e, and the plug length b. The experimental duration time of perforation is given for those cases where it was measured. The results of calculations for the final velocity and the duration time based on the analysis of[1] are also given in Table 3.

The analysis of[1] was also used to calculate final velocities and duration times for a number of the experiments reported in[3]. The details of the geometry of perforation, D and b, are given in[3] while values for e and μ necessary for the calculations were based on results obtained in the present tests. A high speed camera was used in[3] to obtain the duration time of perforation. Table 4 summarizes the experimental and calculated results for these cases.

Table 4. Comparison between test results of Goldsmith and Finnegan[3] and calculations based on[1]

Projectile dia. (mm)	Target material	Target thickness (mm)	Measured velocity (m/sec) Initial (V_i)	Final (V_f)	Computed final velocity (m/sec)	Contact duration Computed (μsec)	Exper. (μsec)
6·35	2024-T3AL	3·18	870	685	595	8·2	8·3
6·35	2024-T3AL	3·18	2610	2230	1937	2·1	2·7
6·35	2024-T4AL	6·35	870	457	411	16·3	10·3
6·35	2024-T4AL	6·35	2540	1900	1499	4·2	4·6
9·52	2024-T4AL	6·35	905	688	566	14·0	—
9·52	2024-T4AL	6·35	2420	1775	1681	4·2	5·5
6·35	1020 steel[a]	6·35	900	0	204†	33·2	13·5
6·35	1020 steel[a]	6·35	2620	915	859	6·8	5·8
6·35	1020 steel[b]	6·35	1475	219	343	15·8	—
6·35	1020 steel[b]	6·35	2115	722	535	10·3	—
6·35	4130 steel	6·35	885	0	0	10·5	8·3
6·35	4130 steel	6·35	1530	210	203	20·0	—
6·35	4130 steel	6·35	1620	358	273	22·2	17·2
6·35	4130 steel	6·35	1890	537	391	15·9	11·0
6·35	4130 steel	6·35	2145	656	487	12·5	—
6·35	4130 steel	6·35	2490	864	599	10·2	—
6·35	4130 steel	6·35	2640	894	646	9·2	5·8

† Close to ballistic limit. [a] Small grain size. [b] Large grain size.

DISCUSSION OF RESULTS

A review of the experimental and calculated final velocities and duration times listed in Tables 3 and 4 indicates fairly good overall agreement between the sets of results. The calculations were based on measured values of the geometric parameters of perforation: D_1, D_3, e and b. The need for empirical data in the application of the analysis is limited, however, since extensive tests have shown that D_{avg} and b are linear functions of the plate thickness for a particular projectile and target material over a moderate range of velocities, Fig. 9. This would mean that D_{avg} (or D_1 and D_3) and b could be obtained from a few tests and the results extrapolated for other plate thicknesses and projectile velocities. The analytical determination of D and b from basic considerations would require the solution of difficult problems which seem to be capable of solution only by complicated numerical

techniques using computers. It is interesting to note that the ratio b/h does not vary significantly for various projectiles and materials. For most of the present tests b/h ranged from 0·80 to 0·85 for mild steel and the various steel alloys and from 0·68 to 0·75 for aluminum and aluminum alloy 6061-T6 with a few tests falling outside these ranges.

As noted in the previous section, the value of the parameter e used in the calculations was obtained from photographs of etched perforated plates. This was not done for all cases since the value of e did not change significantly for similar tests, i.e. for a given projectile and slightly varying target plate thicknesses of similar material. Values for e could also be deduced from analyses of Chou[4] and of Thomson[5]. For example, the value of e calculated from Thomson's analysis for the case of a 0.22 in. bullet perforating a 5 mm thick 6061-T6 aluminum plate is 1·35 mm while post experimental examination gave $e = 1{\cdot}5$ mm. For the case of a 9 mm bullet perforating a 6·35 mm plate of the same alloy, the analysis[5] leads to $e = 1{\cdot}6$ mm while the experiment showed $e = 2{\cdot}0$ mm. The analyses of[4 or 5], or a limited number of tests, could therefore be used to determine the width of the shear zone.

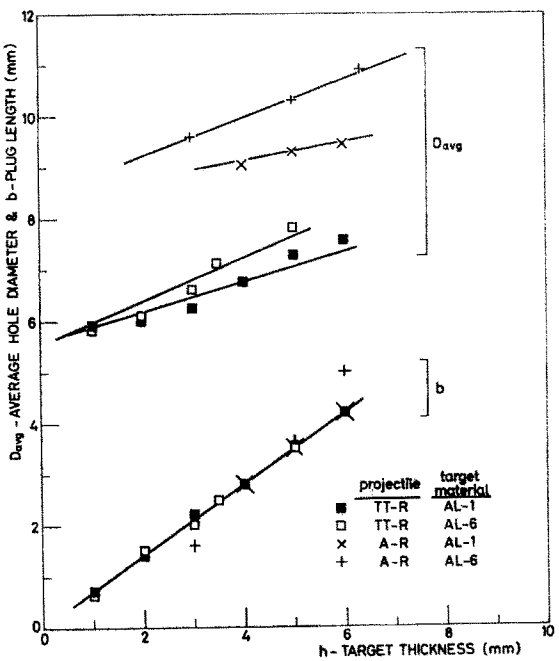

Fig. 9. Dependence of average cavity diameter D_{avg} and plug length b on the thickness of commercially pure aluminum and aluminum 6061-T6 target plates after perforation by TT.-R. and A.-R. projectiles.

The strength properties of the target material that are factors in the analysis[1] are the compressive strength σ_c, the shear strength τ, and the failure strain in shear γ_f. The alloys used as target plates in this program, aluminum alloy 6061-T6, and the high strength steels are relatively rate insensitive[6–8] to moderately high strain rates ($\sim 10^3 \text{sec}^{-1}$) but tend to be quasi-viscous at very high rates ($\sim 10^5 \text{sec}^{-1}$)[9–12]. Commercially pure aluminum is slightly more rate dependent at moderately high rates and becomes more sensitive (quasi-viscous) at the very high rates. Mild steel has appreciable rate sensitivity and it becomes very sensitive at strain rates above 10^3sec^{-1}. The material strength properties listed in

Table 2 were obtained at relatively slow rates in a standard testing machine (quasi-static). The ultimate strength values obtained in these tests were used as σ_c in the equations since the actual compressive strain rates would not be very high and the ultimate stress in compression is not a particularly rate sensitive property for these materials. The quasi-static ultimate shear stress listed in Table 2 was taken to be τ_0 in the equation for the dynamic ultimate shear stress, equation (15) of[1], namely,

$$\tau = \tau_0 + \mu\dot{\gamma}$$

where μ is the coefficient of viscosity and $\dot{\gamma}$ is the shear strain rate. The latter is taken to be the instantaneous velocity of the combined projectile and added mass, V, divided by the width of the shear zone e. The present tests can be considered as experiments for determining μ and values were chosen so that the calculated results would best fit the test data. These were 10, 8 and 10 g sec/cm^2 for aluminum alloy, commercially pure aluminum, and mild and alloy steel respectively. These are reasonably consistent with other experimental data[9–12] where μ varied from 7 to 20 g sec/cm^2 for aluminum and aluminum alloy and was about 20–28 g sec/cm^2 for steel.

The value of the failure strain γ_f was taken to be 0·20 for all the target materials which is a good average for available test data for steels and aluminum alloys tested at moderately high strain rates and agrees with examination of the photomicrographs of the present results. The failure strain is, moreover, an insensitive parameter in the final results.

As has been noted, the agreement between the calculated final velocities and duration times based on[1] and those obtained experimentally is fairly good. The best agreement is for the tests with the 0·22 in. and 9 mm caliber bullets (TT.-R. and A.-R.) on target plates of commercially pure aluminum and 6061-T6 aluminum alloy. The agreement is not so good for the other projectiles and the steel alloy target plates where the calculated final velocities are about 15–25 per cent lower than the experimental measurements. Part of this discrepancy seems to be due to the experimental difficulty of accurately measuring the final velocity when target fragments were propelled at higher velocities than that of the

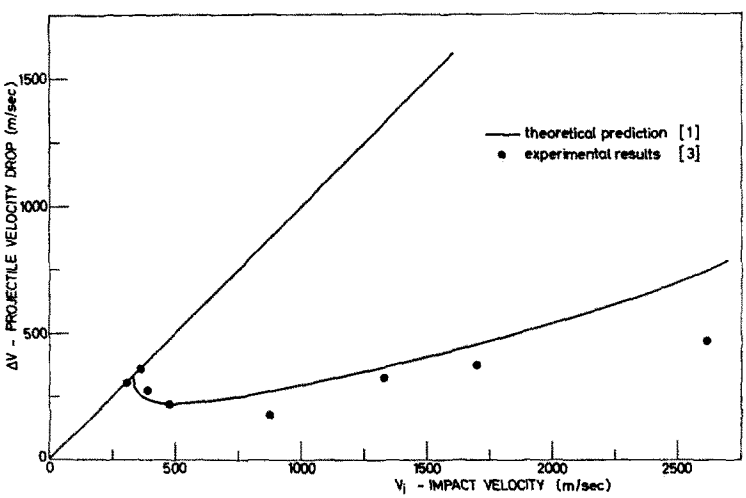

Fig. 10. Projectile velocity drop as a function of initial velocity: 1/4 in. steel spherical projectile perforating 2024-T3 aluminum plate 1/8 in. thick. Comparison between experimental results of [3] and theoretical predictions[1].

combined projectile and plug. The analytical treatment is, of course, a simplified one and it is difficult to evaluate the effect of the various idealizations on the final results.

The calculations do show an interesting and important phenomena observed experimentally when the impact velocity is close to the ballistic limit. The velocity drop $\Delta V = V_i - V_f$ (difference between impact and final velocity) generally increases with increasing impact velocity. However, ΔV decreases for initial velocities slightly above the ballistic limit value. This was observed in the present tests and in those of[3]. This effect corresponds to the general observation that the final velocity of a bullet that perforates a plate is never very small but is a significant percentage (about 15–20 per cent) of the initial velocity. The reason for this effect, as discussed in[1], seems to be that the force and impulse acting during the final steps of the perforation process are relatively high. The details of the last steps of perforation are also sensitive to small variations of the various parameters, especially the impact velocity, which is the reason for the relatively large scatter of both experimental and calculated results for velocities slightly above the ballistic limit. A comparison of calculated final velocities with those obtained in some of the tests reported in[3] is shown in Fig. 10. The calculated results do show the drop of ΔV with increasing V_i as indicated by the test results.

SUMMARY

The results of this experimental program show that the analytical model developed for the perforation process[1], can provide good predictions on post-perforation velocities and duration times. The most important improvement to the analytical treatment seems to be the determination of the geometry of the perforation by direct considerations rather than by the empirical methods presently used. The analysis does indicate a number of important characteristics of ballistic perforation shown by the experimental program.

Acknowledgements—The authors are very grateful to Mr. S. Pinkesfeld and to Mr. M. Gonen for their assistance with the experimental work. The authors also wish to express their appreciation to Mr. D. Cohen for his assistance in preparing the computer programs.

REFERENCES

1. J. Awerbuch and S. R. Bodner, Analysis of the mechanics of perforation of projectiles in metallic plates. MED Report No. 40, May 1973, Dept. of Materials Engineering, Technion, Haifa, Israel; *Int. J. Solids Struct.* **10**, 671–684 (1974). also Int. J. Solids Structures, 1974, this issue, preceding paper.
2. J. Awerbuch, A mechanics approach to projectile penetration. *Israel J. Tech.* **8**, 375–383 (1970).
3. W. Goldsmith and S. A. Finnegan, Penetration and perforation processes in metal targets at and above ballistic velocities. *Int. J. Mech. Sci.* **13**, 843–866 (1971).
4. P. C. Chou, Perforation of plates by high speed projectiles. *Developments in Mechanics*, edited by J. E. Lay and L. E. Malvern, Vol. 1, pp. 286–295. North-Holland Publishing Co., Amsterdam (1961).
5. R. G. Thomson, Analysis of hypervelocity perforation of a viscoplastic solid including the effects of target-material yield strength. NASA TR R-221 (1965).
6. T. Nicholas and J. D. Campbell, Shear-strain-rate effects in a high-strength aluminum alloy. *Exp. Mech.* **12**, 441–447 (1972).
7. C. J. Maiden and S. J. Green, Compressive strain-rate tests on six selected materials at strain rates from 10^{-3} to 10^{4} in/in/sec. *J. Appl. Mech.* **33**, 496–504 (1966).
8. D. L. Holt *et al.*, Strain-rate dependence of flow stress in some aluminum alloys. *Trans. ASME* **60**, 152–159 (1967).
9. A. R. Dowling, J. Harding and J. D. Campbell, The dynamic punching of metals. *J. Inst. Metals* **98**, 215–224 (1970).
10. W. G. Ferguson, A. Kumar and J. E. Dorn, Dislocation damping in aluminum at high strain rates. *J. appl. Phys.* **38**, 1863–1869 (1967).

11. M. F. Kannigen, A. K. Mukherjee, A. R. Rosenfield and G. T. Hahn, The speed of ductile-crack propagation and the dynamics of flow in metals. *Mechanical Behavior of Materials Under Dynamic Loads*, pp. 96–133. Springer, New York (1968).
12. J. D. Campbell and W. G. Ferguson, The temperature and strain-rate dependence of the shear strength of mild steel. *Phil. Mag.* **21**, 63–82 (1970).

Абстракт—В настоящей работе описана экспериментальная программа перфорации баллистическим оружием металлических пластин. Использовались три типа ружей и различные стальные и алюминиевые мишенные пластины. Измеряли исходные и послеперфорационные скорости и в некоторых случаях продолжительность перфорации. Во время процесса перфорации делали высокоскоростные фотоснимки и рассматривали сечения перфорированных мишенных пластин. Анализ физического процесса перфорации, послужил обоснованием аналитического рассмотрения, приведенного в связанной с настоящей работой статье. Результаты эксперимента, т. е. послеперфорационные скорости и продолжительность, хорошо совпали с прогнозом ассоциированного анализа.